Applied Geomatics
https://doi.org/10.1007/s12518-018-0241-3

ORIGINAL PAPER

Code multipath analysis of Galileo FOC satellites by time-frequency representation

Umberto Robustelli [1] · Giovanni Pugliano [1]

Received: 13 March 2018 / Accepted: 5 September 2018

Abstract
Galileo is currently in full operational capability (FOC) phase with 18 FOC satellites. The purpose of this paper is to investigate the multipath performance of Galileo FOC signals E1, E5a, E5b, and E5. With the advent of FOC satellites, assessing the multipath behavior of Galileo FOC signals is becoming one of the greatest interests for the user's community. In fact, the reduction of multipath has been one of the main criteria on which the Galileo signals have been designed. We analyzed data over three different days from six International GNSS Service (IGS) stations located at different latitudes, for all visible Galileo satellites. This is one of the first studies to present experimental results for the multipath of Galileo signals transmitted by FOC satellites since they started to operate in 2015. Code multipath was estimated using code-minus-carrier (CMC) and pseudorange multipath (MP) methods. The study involves a comparison with the GPS signals, showing results of multipath performance as function of satellite elevation. A time-frequency representation, based on the use of continuous wavelet transform (CWT), was performed to rigorously account for the presence of multipath. The expectations of FOC satellites to lead to a multipath reduction have been verified: the E5 signal shows the highest suppression of multipath as compared to the other Galileo and GPS signals and it is almost independent from the satellite elevation. An assigned FOC satellite showed a lower frequency multipath compared to a GPS satellite at the same azimuth and elevation, which is in line with a lower Galileo satellite elevation rate.

Keywords Galileo FOC satellites · Time-frequency analysis · Scalogram · Continuous wavelet transform · Multipath · Code-minus-carrier · Pseudorange multipath observable

Introduction

Galileo, the European Global Navigation Satellite System, is currently (March 2018) in its full operational capability (FOC) phase; 18 FOC satellites were launched by the end of 2017, the first two of which—PRN 14 and PRN 18—launched into anomalous elliptical orbits, 11 operational and four are currently being tested before being commissioned for operational service. When the experiment has been carried out on November–December 2016, 13 satellites, including three in-orbit validation (IOV) launched in 2011 and 2012 and ten FOC, were marked as healthy. The Galileo satellites currently transmit four signals: E1, E5a, E5b, and E5. Each one of them has two different components, the data and pilot channels, combined and transmitted by using the composite binary offset carrier (CBOC) modulation. The pilot component is not modulated by a navigation data stream but only contains ranging code, subcarrier, and secondary code. The E1 signal is transmitted in the frequency band (1559–1591 MHz) and it provides the integrity navigation message (I/NAV). The Galileo E5 signal consists of the signals E5a and E5b and is transmitted in the frequency band 1164–1215 MHz. The E5a signal provides the navigation message (F/NAV) while the E5b signal provides the I/NAV message; both of them are freely accessible. The signals E5a and E5b are modulated onto the E5 carrier frequency using the alternative binary offset carrier modulation AltBOC(15,10) (OS SIS ICD 2015). Receivers can track E5a and E5b as two independent signals at center frequencies of 1176.45 MHz and 1207.14 MHz respectively or as one signal centered at 1191.795 MHz to achieve better performance from E5. The AltBOC modulation and advantages of tracking Galileo signal E5 are discussed in several papers, see Tawk et al. (2011).

✉ Umberto Robustelli
umberto.robustelli@uniparthenope.it

[1] Department of Engineering, Parthenope University of Naples, Naples, Italy

Published online: 12 September 2018

Multipath is still one of the greatest challenges in GNSS positioning, which can be inaccurate from a few decimeters or even some meters in severe environments such as urban canyons. The reduction of multipath effects by optimizing the signal definition and the guarantee of coexistence and interoperability with existing systems have been the main design criteria for the new Galileo signals.

Due to the new signal features, during the early stages, authors have focused their studies on the techniques for the acquisition, on the specific code discriminators and code tracking architecture especially tailored to the CBOC modulated signals. Julien et al. (2004) focused on the availability of both the data and pilot channels developing a tracking method that showed good resistance to noise and multipath. Borio and Lo Presti (2008) proposed two strategies for the acquisition of Galileo E1 open service (OS). Zhang and Lohan (2011), using synthetic data, showed that the tracking performances in multipath environments with E5a signals are better than those with E1 signals most of the time, especially with a high carrier-to-noise ratio.

The signals transmitted by the Galileo in-orbit validation element (GIOVE) satellites were tested by Simsky et al. (2006, 2008). They estimated the Galileo code multipath by using the pseudorange multipath observable, a linear combination of dual frequency pseudorange and carrier phase measurements (see Hofmann-Wellenhof et al. 2001; Leick 2004). Their results showed that the E5 signal has the highest multipath suppression when compared to other signals with a lower value of multipath error of about 20 cm. Changsheng et al. (2016) focused their research on the Galileo signal multipath performance in the measurement domain, using real data recorded in May 2014 from Galileo IOV satellites E11 and E12. They studied multipath through the zero-baseline double difference and double frequency approach, finding a root mean square (RMS) multipath error for code observations of 17 cm for Galileo IOV signal E1, 27 cm for E5a and E5b, 10 cm for E5 respectively. Diessongo et al. (2014) used the code-minus-carrier (CMC) observable coming from the GIOVE and Galileo IOV satellites in order to compare code noise between Galileo signals E1 and E5. These studies did not analyze the FOC satellites as they refer to the GIOVE, mainly designed for testing the technologies in orbit such as the satellite frequencies, and IOV satellites, fully representative from a frequency and modulation point of view, with a lower transmit power than FOC satellites.

The multipath error central frequency is proportional to the orthogonal distance from the antenna to the reflecting plane, inversely proportional to the wavelength, and depends on the satellite elevation angle. As the satellite is continuously moving, multipath frequency is time-variant. Thus, multipath is a non-stationary random process with a time-varying mean, a time-varying variance, and a time-variant power spectrum: some spectral components are present only in limited time intervals. Fourier analysis provides excellent frequency resolution but is not suitable to analyze the multipath error since it can only be applied to stationary signals and does not allow to extract the time instant in which the phenomenon occurs. Thus the wavelet analysis of multipath data becomes a key tool to achieve an in-depth estimation, identifying the time instant when multipath occurs and its central frequency.

There are still no studies in literature regarding the multipath time-frequency analysis leading to scalogram representation of Galileo's real data, although the use of wavelets for GPS multipath analysis has been applied in several works (Souza and Monico 2004; Satirapod and Rizos 2005). A comprehensive state of the art account could be found in Pugliano et al. (2016) where a new technique is developed and employed to characterize the CMC GPS L1 residuals in the time-frequency plane.

The analysis that we conducted was mainly intended to assess the multipath performance of Galileo FOC satellites using real datasets from six stations all equipped with choke-ring antennas of the IGS network (Dow et al. 2009), located at different latitudes in sites where it is expected to be a low-multipath environment in conformity with IGS site guidelines (http://kb.igs.org/hc/en-us/articles/202011433-Current-IGS-Site-Guidelines). We evaluated and analyzed four FOC code observables—E1, E5a, E5b, E5—with the aim of contributing towards understanding how the code multipath error is impacting on the Galileo FOC signals.

It is one of the first studies to present experimental results for the multipath of Galileo signals transmitted by FOC satellites since they started to operate in 2015. Circiu et al. (2017) analyzed the performance of signals from the Galileo satellites in the E1 and E5a frequency bands showing that the multipath level of these signals is smaller than that of GPS L1. Zaminpardaz and Teunissen (2017) analyzed the code multipath performance of FOC satellites and the differences between Galileo IOV and FOC signals in terms of carrier-to-noise density ratio C/N_0 measurements. They showed that the E5 signal has significantly smaller values with respect to that of the other Galileo signals, with low dependency both on the receiver/antenna type and the multipath environment. Sosnica et al. (2018) and Paziewski et al. (2018) focused their studies on the PRN 14 and PRN 18 Galileo FOC satellites launched into incorrect elliptic orbital planes. The firsts analyzed the quality of the Galileo orbits using SLR data, while the seconds evaluated the performance of the coupled Galileo-GPS instantaneous medium range positioning.

Our paper involves a comparison with the GPS signals, showing results on multipath performance as function of satellite elevation. A time-frequency representation, based on the use of the continuous wavelet transform (CWT), was performed to rigorously account for the presence of multipath.

Table 1 Galileo signal frequencies and maximum carrier phase tracking error due to multipath

Signal	Freq. (MHz)	M_ϕ (cm)
E1	1575.42	4.8
E5a	1176.45	6.4
E5b	1207.14	6.2
E5	1191.795	6.3

Methodology

Two different observables are adopted to achieve code multipath estimation: the code-minus-carrier (CMC) (Braasch 1996) and the pseudorange multipath observable (MP) (Defraigne and Bruyninx 2007; Seepersad and Bisnath 2014). These observables are both linear combination of code and carrier phase observables.

Code-minus-carrier

CMC is obtained by subtracting, in the range domain, the carrier phase from the code observable at every epoch t for each satellite:

$$\begin{aligned} CMC = P - \lambda\phi = {} & \rho + c(\delta t_r - \delta t^s) + d\rho + I + T + b_P \\ & + B_P + M_P + \varepsilon_P + -\rho - c(\delta t_r - \delta t^s) - d\rho \\ & + I - T - b_\phi - B_\phi - M_\phi - \varepsilon_\phi - \lambda N \end{aligned} \quad (1)$$

where P is the code observable, λ is the wavelength at the selected frequency, ϕ is the carrier phase observable in units of cycles, ρ is the geometric range between the receiver and the satellite, c is the speed of light, δt_r is the receiver clock error, δt^s is the satellite clock error, $d\rho$ is the orbital error of the satellite, I is the delay or advance due to the ionosphere, T is the delay due to the troposphere, b_P is the code satellite hardware bias, B_P is the code receiver hardware bias, M_P is the code multipath error, ε_P is the code measurement noise, M_ϕ is the code multipath error, b_ϕ is the carrier phase satellite hardware bias, B_ϕ is the carrier phase receiver hardware bias, ε_ϕ is the carrier phase measurement noise, N is the integer carrier phase ambiguity. Note that in (1) the errors common to both the code and carrier phase measurements (i.e., satellite and receiver clock offsets, orbital error, troposphere delay) are removed because of the differencing. The terms remaining are twice the ionospheric error, the carrier phase integer ambiguity, the satellite and receiver hardware biases, the multipath error associated with code and carrier phase measurements and the combined receiver noise $\varepsilon_{P,\,\phi}$. Thus CMC is used to approximate the multipath (including carrier phase multipath and measurement noise) which is given as

$$M_P - M_\phi + \varepsilon_{P,\phi} \cong CMC - 2I - b_P - B_P + b_\phi + B_\phi + \lambda N \quad (2)$$

For all GNSS systems and in particular for the Galileo system (de Bakker et al. 2009) and for the GPS (El-Rabbany 2002; Braasch 1996) the carrier phase multipath error and receiver noise are assumed to be almost an order of magnitude smaller than the code multipath error and code receiver noise respectively. The maximum carrier phase tracking error due to multipath interference from a reflected signal of the same amplitude as the direct signal is a quarter of a wavelength (Petovello and Groves 2013) thus the carrier phase multipath error M_ϕ can reach a maximum value of one quarter of a cycle, corresponding to 6.3 cm for signal E5 (Table 1).

Ionospheric delay I is slowly varying with a time correlation of 15–30 min (Mannucci et al. 1997), corresponding to a frequency spectrum lower than 0.1 mHz (Bartone and Zhang 2005). It can be modeled as constant (Bartone and Zhang 2005) or a second order polynomial can be used to better represent its slow variations (de Bakker et al. 2012).

The receiver and satellite hardware biases are temporary stable (Hakansson et al. 2017); thus, they can be removed.

Regarding the ambiguity term, several authors (Aram et al. 2007; Blanco-Delgado and de Haag 2011; de Bakker et al. 2009) considered it as a bias because it is constant over time in the absence of cycle slips or it has a step function if a cycle slip occurs. In this study only datasets without cycle slips are used, there detection is performed using TEQC software (Estey and Meertens 1999).

Thus ionosphere, ambiguity and hardware biases can be estimated by taking a moving average. The moving average is an excellent smoothing filter, effective in reducing random noise and despite its bad low-pass filter properties (Smith 1999), it achieves good results as a bias remover (Yates and Lyon 2008). Thus, by using the moving average filter (3), we achieve two results: the estimation of the ambiguity and ionospheric error and the reduction of receiver noise. The ambiguity term and the ionospheric error are estimated by taking the centered moving average of the $\overline{\mathrm{CMC}}$ on $2k+1$ samples from sample $-k$ to sample k as reported in (3):

$$\overline{\mathrm{CMC}} = \frac{\sum_{i=-k}^{k} \mathrm{CMC}_i}{2k+1} \quad (3)$$

where $2k+1$ is the number of samples. Each average consists of $2k+1$ consecutive samples. The larger the value of k, the flatter and smoother the output will be. The cut-off frequency f_{co} of moving average filter can be express as $0.443/T_w$, where T_w is the duration of the window chosen. Moving average was carried out with $k = 1000$ corresponding to a cut-off frequency of 0.4 mHz. Finally, $\mathrm{CMC}_{\mathrm{res}}$ can be calculated as reported in (4)

$$\mathrm{CMC}_{\mathrm{res}} = \mathrm{CMC} - \overline{\mathrm{CMC}} = M_P - M_\phi + \varepsilon_{P,\phi} + \varepsilon_{\mathrm{res}} \quad (4)$$

Table 2 IGS station used

Id	City	Country	Latitude (Deg)	Longitude (Deg)	Height (m)	Receiver	Antenna
EBRE	Roquetes	Spain	40° 49' 15"	0° 29' 23"	107.3	LEICA GR50	LEIAR25.R4
HARB	Pretoria	South Africa	− 25° 53' 13"	27° 42' 26"	1558.1	Trimble NETR9	TRM59800.00
JFNG	Jiufeng	China	30° 30' 56"	114° 29' 27"	71.3	Trimble NETR9	TRM59800.00
NKLG	Libreville	Gabon	0° 21' 14"	9° 40' 19"	31.5	Trimble NETR9	TRM59800.00
RGDG	Rio Grande	Argentina	− 53° 47' 9"	− 67° 45' 5"	32.4	Trimble NETR9	TRM59800.00
YEL2	Yellowknife	Canada	62° 28' 52"	− 114° 28' 51"	181.0	Sept. POLARX4TR	LEIAR25.R4

where ε_{res} represents the residual error due to the removal of ionosphere, ambiguity and hardware biases.

Pseudorange multipath observable

The pseudorange multipath observable is a linear combination of dual frequencies code and phase measurements. It is used to characterize the magnitude of the pseudorange multipath and noise for any GNSS system by the TEQC software (Estey and Meertens 1999). Pseudorange multipath can be estimated by equations (Seepersad and Bisnath 2014)

$$\begin{aligned} \mathrm{mp}_i &= P_i - \left(1 + \frac{2}{\alpha - 1}\right)\lambda_i\phi_i + \left(\frac{2}{\alpha - 1}\right)\lambda_j\phi_j \\ &= M_{P_i} + \varepsilon_{P_i} + K + Id \end{aligned} \tag{5}$$

$$\begin{aligned} \mathrm{mp}_j &= P_j - \left(\frac{2\alpha}{\alpha - 1}\right)\lambda_i\phi_i + \left(\frac{2\alpha}{\alpha - 1}\right)\lambda_j\phi_j \\ &= M_{P_j} + \varepsilon_{P_j} + K + Id \end{aligned} \tag{6}$$

where the subscripts i and j denote two different bands, mp_i and mp_j are the estimates of the code multipath error, P_i and P_j are the code observables, λ_i and λ_j are the wavelengths, ϕ_i and ϕ_j are the carrier phase observables in units of cycles, M_{P_i} and M_{P_j} are the code multipath, ε_{P_i} and ε_{P_j} are the receiver noise error of the code measurements, K is a constant term associated with phase ambiguities, Id is a term associated with instrumental delays and $\alpha = (f_i/f_j)^2$ with f_i frequency on i band and f_j frequency on j band. Using the multi-frequency Galileo signals, several values of j are possible. According to (Simsky et al. 2006) the particular selection of j does not significantly affect the results. In contrast recently Zaminpardaz and Teunissen (2017) shown that when f_i is the frequency of E5 one should avoid selecting f_i as frequency of E5a or E5b, so we according to them to obtain mp_5 we chose E1 as f_j frequency.

Equations (5) and (6) contain pseudorange multipath, noise and errors due to phase ambiguities, instrumental delays, and phase wind up. We want to highlight that unwanted effects (namely receiver biases and ambiguities) are supposed to be constant. Moreover, in the case of a receiver with fixed coordinates, the carrier phase wind up effect is only due to the satellite orbital motion. For short periods of observation, this effect is typically ignored because antenna rotation results in a drift of receiver clock estimate (Soloviev et al. 2007).

As stated before, ambiguity can be estimated by using moving average taken on 1000 samples. Finally, multipath can be obtained by subtracting its moving average as follows:

$$\mathrm{MP}_j = \mathrm{mp}_j - \overline{\mathrm{mp}_j} \tag{7}$$

where $\overline{\mathrm{mp}_j}$ is the moving average of mp_j. This technique removes the ionosphere error by using iono-free carrier measurements. The noise introduced is at millimeter level, well below code thermal and multi-path noise; moreover, the noise

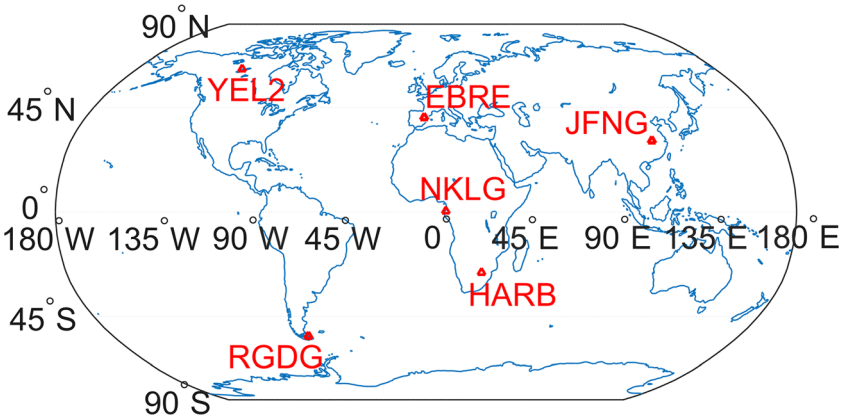

Fig. 1 Stations positions

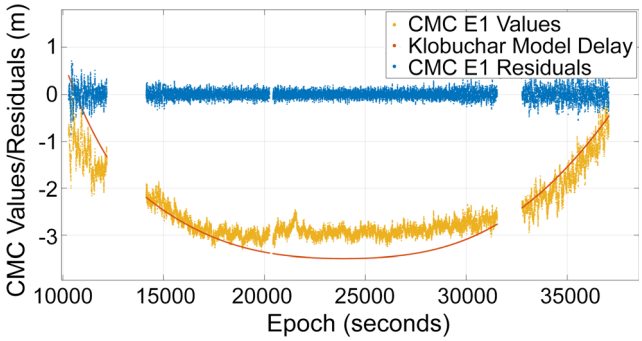

Fig. 2 CMC (blue) and CMC residuals (yellow) of PRN 01 satellite for E1 signal, plotted versus time on DOY 339 in YEL2 site. The red line represents the Klobuchar model ionospheric delay translated for better readability

level of Galileo code is lower than that of GPS, hence justifying the use of this technique.

As stated before both CMC residual and pseudorange multipath observable are non-stationary random processes, they have time-variant spectra with some spectral components present only in limited time intervals. Thus, in order to achieve a good time-frequency analysis, a continuous wavelet transform is applied. As a result of this analysis, a scalogram that is a time-scale representation of spectrum is obtained. The difference between the two techniques lies in the fact that the CMC observable can also be formed by using data acquired by a single frequency receiver, while the MP observable can only be obtained by a dual frequency receiver.

Data processing

We have processed the measurements captured by six stations of the IGS, placed at different latitudes and Earth's hemispheres. The analysis was carried out on all currently available Galileo signals from all visible satellites. The stations' coordinates are listed in Table 2 and their global positions are shown in Fig. 1. These sites are expected to be in a low-multipath environment as IGS sites guidelines impose. The experiment was carried out using RINEX 3.0 file data collected at 1 Hz rate by three different antenna-receiver couples. The first couple, placed in the YEL2 site, is made up by a Septentrio Polarx4TR receiver fed by the LEIAR25.R4 choke-ring antenna; the second one, placed in EBRE, is made up by LEICA GR50 receiver fed by the LEIAR25.R4 choke-ring antenna; the third one, placed in all remaining sites, is made up by a Trimble NETR9 receiver fed by a TRM59800.00 choke-ring antenna as shown in Table 2. All receivers can track Galileo L1 CBOC, E5A, E5B, and E5AltBOC signals simultaneously.

The nominal trajectory followed by the operational Galileo satellites is a circular orbit with a radius of approximately 29,599.8 km equivalent to 23,229 km altitude over the Earth surface (OS SIS ICD 2015). For an ideal Keplerian orbit, the orbital period T is set by (8)

$$T = 2\pi\sqrt{\frac{a^3}{\mu}} \tag{8}$$

$$n{\cdot}T = m{\cdot}D_s \tag{9}$$

Table 3 MNE and MPE PRN 08 satellite multipath error in RGDG site

	CMC		MP	
	MNE (cm)	MPE (cm)	MNE (cm)	MPE (cm)
E1 first peak	− 79.9	61.1	− 80.9	60,9
E1 second peak	− 59.3	61.7	− 60.0	65.6
E5a	− 83.3	92.6	− 82.4	96.3
E5b	− 89.1	84.0	− 95.5	94.9
E5	− 39.5	40.1	− 37.6	41.9

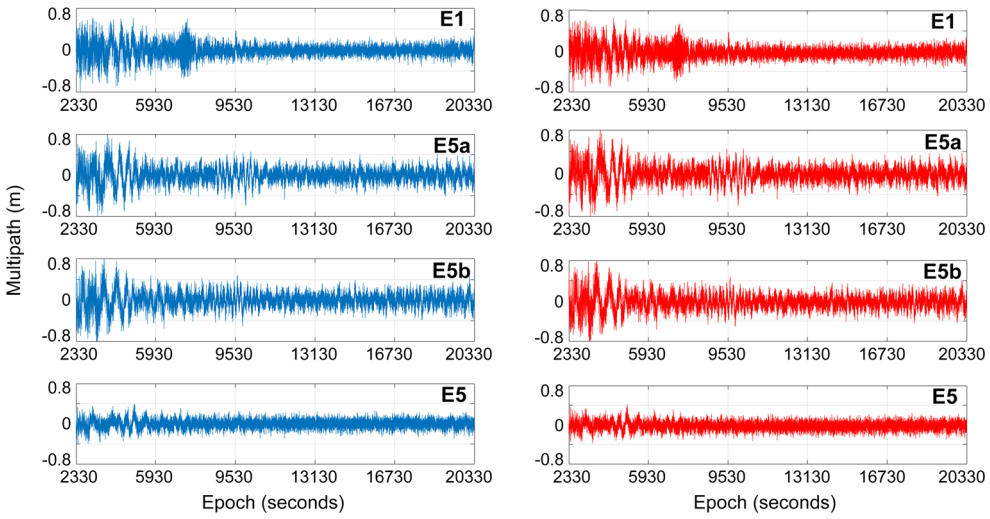

Fig. 3 CMC (left) and MP (right) multipath estimation for signal E1, E5a, E5b, E5 for PRN 08 at site RGDG on DOY 319. CMC and MP estimations give very similar result, so they can be used interchangeably to estimate multipath

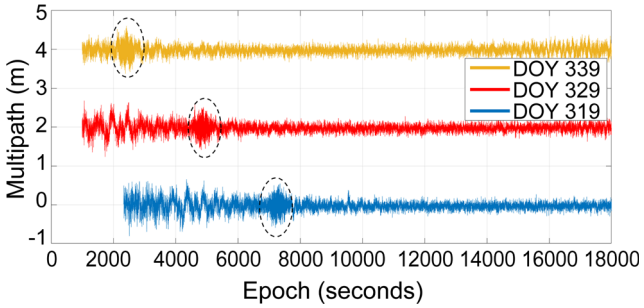

Fig. 4 E1 pseudorange multipath observable for PRN 08 in RGDG site plotted versus seconds of the day for DOY 319 (blue), 329 (red) and 339 (yellow). For better readability, multipath estimates for DOY 329 and 339 are shifted by 2 and 4 m respectively

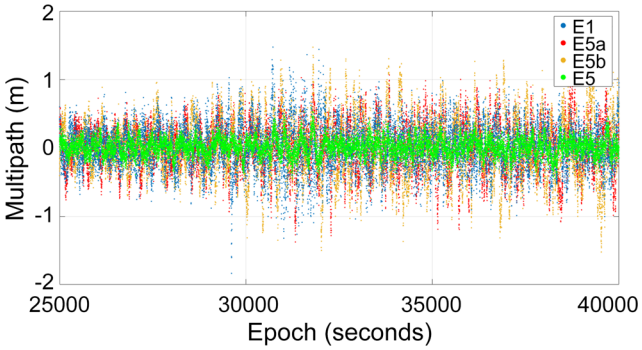

Fig. 6 PRN 30 code multipath data for DOY 339 in NKLG site for E1 (blue), E5a (red), E5b (yellow) and E5 (green) signals

where a is the semi-major axis of the orbit and $\mu = 3.986\,005 \cdot 10^5\ \frac{km^3}{s^2}$ is the product of the universal gravitational constant and the mass of the Earth. Thus Galileo satellites have an orbital period of about 14 h and 5 min. The repeating ground track orbit design can be established by looking for the couple of integer numbers (n, m) that satisfy the equality reported in (9) with the orbital period of $T \approx 14.0782$ h and the sidereal day $D_s = 23.9344$ h. The Galileo satellites have a 10-day ground track repeat cycle every 17 orbits ($n = 17$, $m = 10$). Since a sidereal day is 236 s shorter than a solar day, in the ideal case, each Galileo satellite would appear in its position 39 min and 20 s earlier after 10 days. This is true for all satellites with the exception of PRN 14 and PRN 18 which were left in a non-nominal highly elliptical orbit due to a launch failure. In order to make the satellites usable, a series of orbital maneuvers were done. Nowadays the PRN 14 and PRN 18 satellites have a more circular orbit and overfly the same location on the ground every 20 sidereal days (Navarro-Reyes et al. 2015).

Assuming that the multipath comes from stationary objects and using the same antenna and satellite positions, the multipath error should repeat itself with a difference of approximately 40 min, making it possible for it to be checked by collecting data every ten days (or twenty for PRN 14 and PRN 18) during the same observation period. Thus in order to investigate multipath characteristics of the sites, we choose three DOYs spaced by ten days in order to ensure repeatability of the satellites. Galileo observables (1 Hz data) carried by E1, E5a, E5b and E5 signals, from 0:00 am until 24:00 pm local time on November 14 (DOY 319), November 24 (DOY 329) and December 4 (DOY 339) of the 2016 were analyzed, with the sole exception of the EBRE site, for which data on June 27, 2018 (DOY 178) were analyzed, in order to test a third receiver-antenna couple. A mask angle of 5 degrees was set to exclude the excessively noisy satellites.

According to methodology section, the first step was to rule out the presence of any cycle slips. The next step was to calculate the CMC according to (1), CMC residuals according to (4) and pseudorange multipath observable according to (7) for all signals on DOY 319, 329, 339. Figure 2 depicts the CMC and CMC residuals for the E1 signal of PRN 01 satellite on December 4, 2016 (DOY 339) in YEL2 site. The CMC values, represented in yellow, show a trend that corresponds to the ionosphere effect as confirmed by the overlap with the estimate of the ionospheric delay carried out with the Klobuchar model (red curve). It is evident how this trend shows a slower variation compared to the high-frequency phenomenon due to multipath and noise. The time evolution of the CMC residuals, shown in blue, clearly demonstrates the removal of both the ionospheric delay and the ambiguity term estimated by taking the centered moving average according to (3).

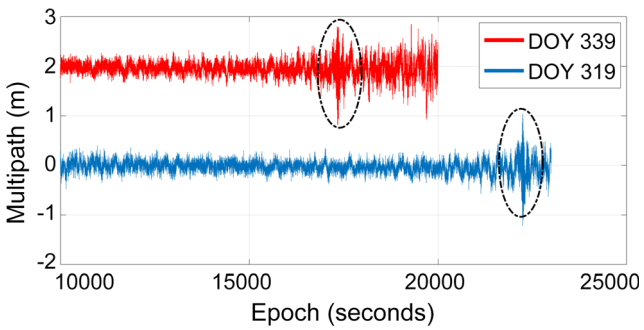

Fig. 5 E1 pseudorange multipath observable for PRN 14 in RGDG site plotted versus seconds of the day for DOY 319 (blue) and 339 (red). For better readability, the multipath estimate for DOY 339 is shifted by 2 m

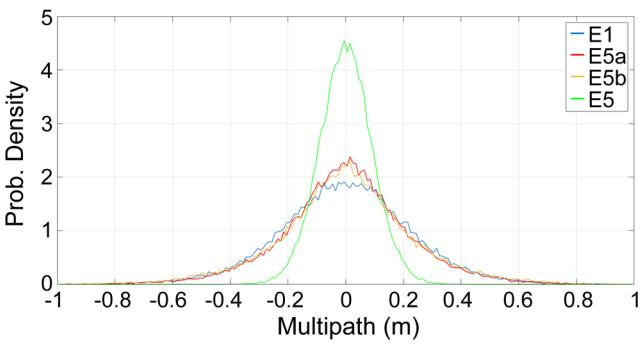

Fig. 7 Sat 30 code multipath probability density curve for DOY 339 in NKLG site for E1 (blue), E5a (red), E5b (yellow), and E5 (green) signals

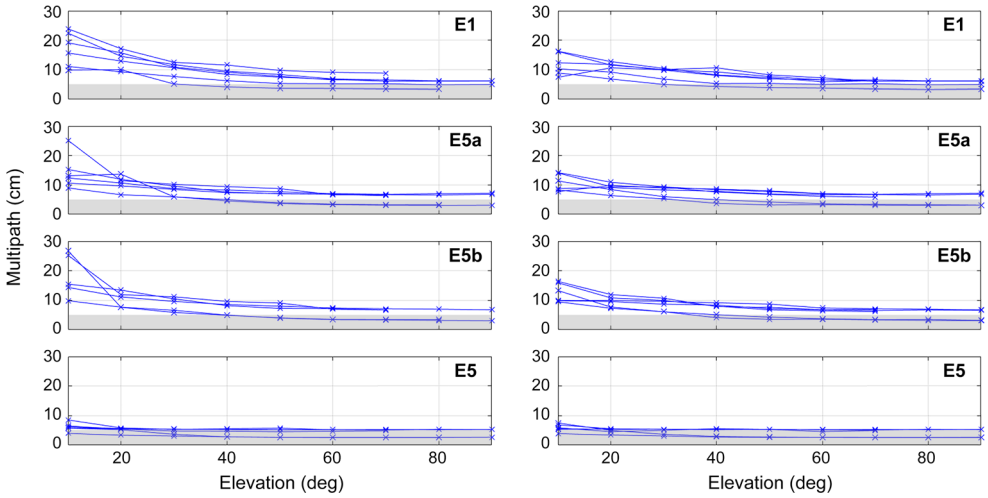

Fig. 8 IOV (left) and FOC (right) satellite code multipath plotted versus elevation

CMC and MP multipath estimations of PRN 08 satellite in RGDG site on November 14, 2016 (DOY 319) are plotted as function of time in the left and in the right column of Fig. 3, respectively.

From Fig. 3, it emerges that CMC (blue) and MP (red) multipath estimations give very similar estimation, this is due to the common moving average taken on 1000 samples. In detail, each signal shows the same peaks at the same time instant in both columns; maximum negative error (MNE) and maximum positive error (MPE) listed in Table 3 confirm this. For this reason, CMC or MP can be used interchangeably to estimate multipath.

A preliminary analysis has been performed in time domain. In Fig. 4, the multipath for E1 frequency transmitted by PRN 08 satellite during DOY 319 (in blue), 329 (in red) and 339 (in yellow) in the Rio Grande (RGDG) site is plotted. The plots confirm that the multipath error peak occurs every ten days with an advance of approximately 2400 s as can be clearly seen from the figure below.

In Fig. 5, the RGDG site multipath for E1 frequency transmitted by PRN 14 satellite, moving on a non-nominal orbit, during DOY 319 (in blue) and 339 (in red) is plotted. In this case, in order to check repeatability and consequently identify code multipath, the analysis must be conducted every 20 days. The figure clearly shows that multipath error peak occurs every 20 days with an advance of approximately 4800 s.

Figure 6 shows the code multipath as a function of time for E1 (blue), E5a (yellow), E5b (red) and E5 (green) signal referred to the PRN 30 satellite on December 4, 2016 (DOY 339) at NKLG site, while Fig. 7 shows their probability density distribution. By observing Fig. 6, it can be noticed that, as expected, E5 signal shows lower multipath code values with respect to the other signals; this is highlighted by Fig. 7 in which the distribution associated with the E5 signal (green) shows the lowest dispersion around the null value.

In order to compare multipath magnitude error in the six stations, multipath was analyzed as a function of the satellite elevation and the carrier-to-noise ratio. In Figs. 8 and 9, IOV and FOC satellites multipath estimations for each site are

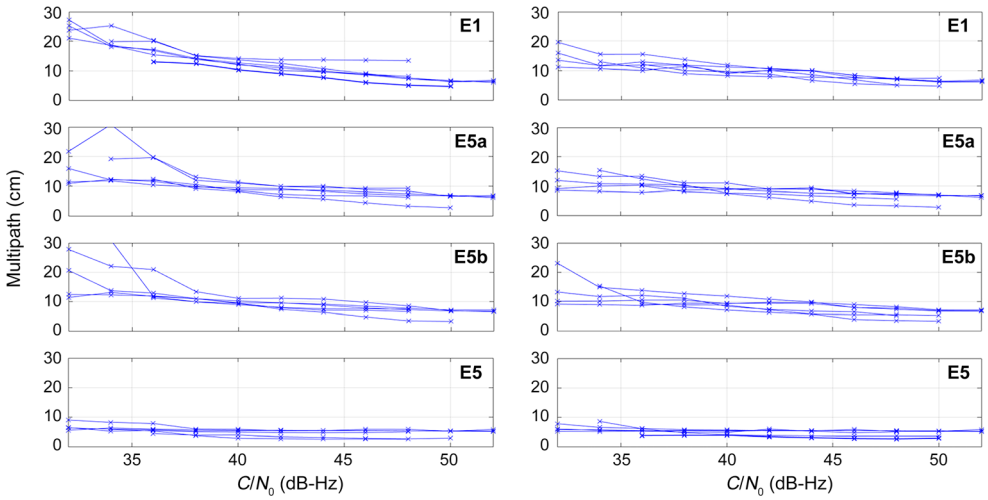

Fig. 9 IOV (left) and FOC (right) satellite code multipath plotted versus C/N_0 ratio

Table 4 FOC satellite code multipath standard deviation on 3 days

Site	std E1 FOC (cm)	std E5 FOC (cm)
EBRE	45.3	39.9
HARB	45.7	33.5
JFNG	81.8	64.6
NKLG	84.9	62.5
RGDG	28.3	19.1
YEL2	49.3	37.7

plotted as a function of the satellite elevation and the carrier-to-noise ratio. The mean multipath errors are computed for elevation bins of 10 degrees and C/N_0 intervals of 2 dB-Hz.

In Fig. 8, code multipath errors on all the frequencies E1, E5a, E5b, and E5 are plotted as a function of elevation angle for the six sites analyzed. The performance of IOV and FOC satellites are shown in the left and right column respectively. Each graph contains six lines representing code multipath for a specific site. It can be noticed that the effect of the site becomes more evident at low elevations. From the figure, it emerges that multipath decreases with increasing elevation angle as expected, with the exception of E5 frequency (shown in the bottom boxes) which appears to be a constant. Two sites (EBRE and YEL2) show code multipath values lower than those of the other four (HARB, JFNG, NKLG, RGDG); in particular, at elevations above 40 degrees, the multipath error for the two aforesaid sites is contained below 5 cm (gray band).

In Fig. 9, code multipath errors are plotted as function of C/N_0. As in Fig. 8, the performance of both IOV and FOC satellites for each site and frequency is depicted. Site dependency disappears starting from a C/N_0 of 40 dB-Hz. The multipath decreases with an increase of C/N_0 with the exception of E5 frequency (shown in the bottom boxes) which appears to be a constant.

The E1, E5a, and E5b signals exhibit very similar code multipath values, especially for FOC satellites. The Galileo E5 signal exhibits the smallest code multipath values for both IOV and FOC. This can be easily understood because when

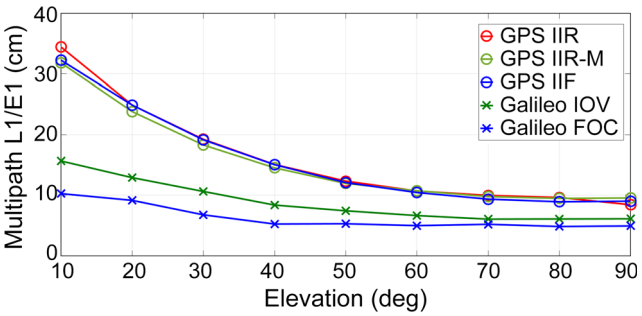

Fig. 10 RGDG Galileo and GPS satellite L1/E1 code multipath plotted versus elevation. E1 Galileo signal has better performance than L1 GPS signal

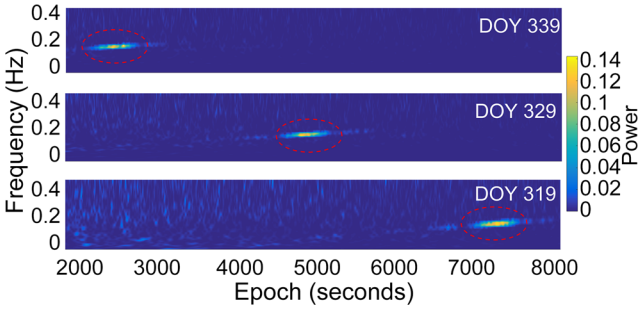

Fig. 11 E1 multipath estimation bump CWT scalogram for the PRN 08 satellite in RGDG site DOY 339 upper box, 329 middle box and 319 lower box. The red circles highlight code multipath

compared to other signals, the E5 has a bandwidth that is wider by at least 51 MHz. To better show the improvement of the E5 signal compared to the E1, Table 4 lists the standard deviations of the code multipath for the two frequencies respectively, calculated on data collected over 3 days for each site.

In Fig. 10, GPS IIR, IIR-M, IIF, and Galileo IOV and FOC satellites median multipath estimations for RGDG site are plotted as a function of the satellite elevation. The median multipath errors are computed for elevation bins of 10 degrees. From the figure it emerges that E1 Galileo signal has better performance as compared to the L1 GPS signal; multipath error decreases with increasing elevation angle as expected. The difference between Galileo and GPS signals becomes smaller at high elevations.

Continuous wavelet transform analysis

In order to obtain a complete characterization of code multipath error, we also need to assess the code multipath central

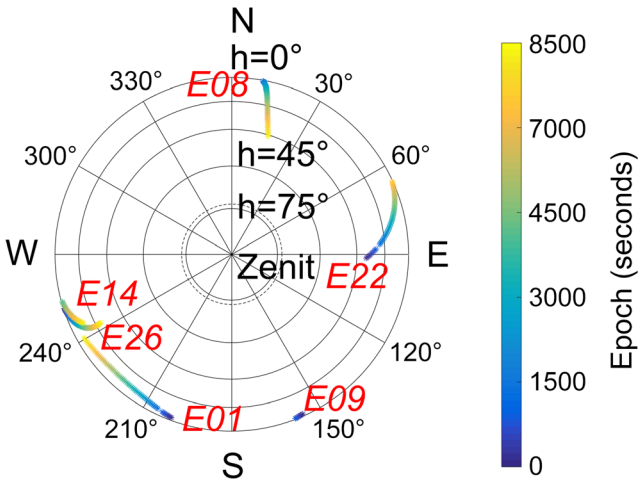

Fig. 12 Sky Plot DOY 319 for time instants in the range 1–8500 s at RGDG site. Each tracked satellite is represented by a color bar. Blue is shown for the start time of observation and yellow is shown for the end time

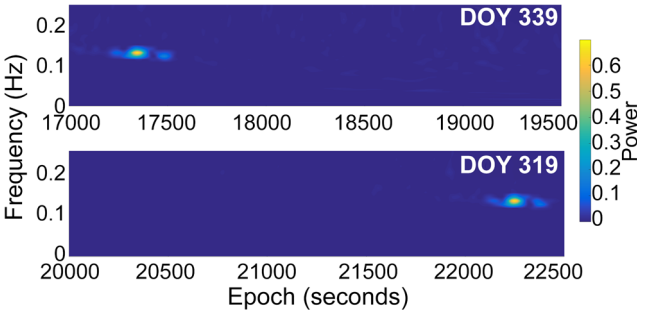

Fig. 13 MP1 multipath estimation bump CWT scalogram for the PRN 14 satellite in RGDG site for DOY 339 (upper box) and 319 (lower box). Here, only 2 days are reported as PRN 14 satellite moves on a different orbit

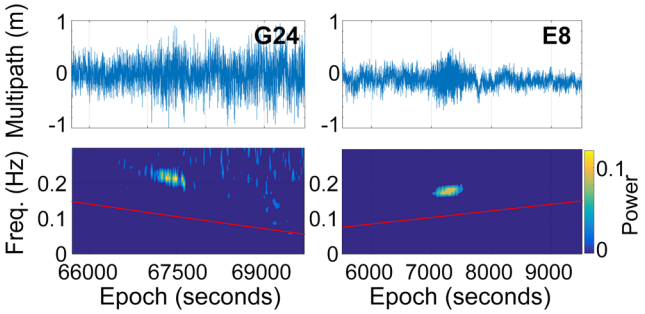

Fig. 15 GPS PRN 24 satellite (left) and Galileo FOC PRN 08 satellite (right) code multipath and bump CWT scalogram at RGDG site for DOY 319. The multipath error was calculated for GPS L1 and Galileo E1 signals. Red lines represent a scaled version of the satellite elevation

frequency. The results reported in Figs. 4, 5, and 6 show the transition from one frequency to another, but they cannot allow us to identify the site-dependent multipath central frequency. With the purpose of investigating this frequency, we applied to CMC and MP observables a well-known time-frequency technique: the wavelet transform. Because it has already been treated in various publications, we will only report the equation and its main features; more details can be found in Pugliano et al. (2016).

The continuous wavelet transform of signal $f(t)$ results in many coefficients C_i, which are a function of scale and position. CWT is obtained by comparing the wavelet function with a section of signal at the start time calculating C_i according to (10), then the wavelet is shifted and the coefficients are calculated until the whole signal is covered. Finally, the wavelet is scaled and the previous steps are repeated. The coefficients C_i, are given as

$$C_i(s,p) = \int_{-\infty}^{+\infty} f(t)\psi^*\left(\frac{t-p}{s}\right)dt \tag{10}$$

Where i indicates the i-th CWT coefficient, ψ^* is the complex conjugate of the mother wavelet function $\psi(t)$, s is the scale, which is used to change the frequency or shape of the wavelet function, and p is the time translation, which is used to shift

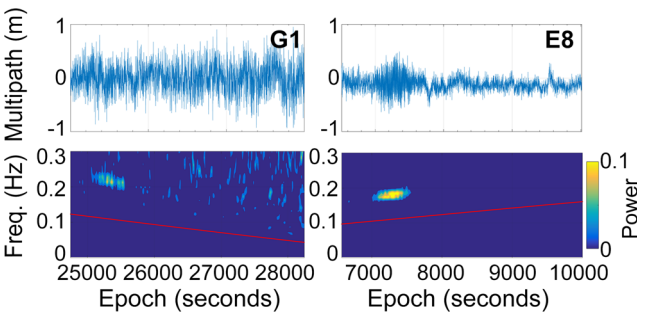

Fig. 14 GPS PRN 01 satellite (left) and Galileo FOC PRN 08 satellite (right) code multipath and bump CWT scalogram at RGDG site for DOY 319. The multipath error was calculated for GPS L1 and Galileo E1 signals. Red lines represent a scaled version of the satellite elevation

the wavelet function to a certain position. The scalogram represents, in the time-scale plane, the percentage of energy for each wavelet coefficient calculated according to:

$$S_{C_i} = \frac{|C_i(s,p)|^2}{\sum_{i=1}^{N}|C_i(s,p)|^2} \tag{11}$$

where S_{C_i} is the percentage of energy associated with CWT coefficient C_i at the scale s at the translation time p. The mathematical definition of the CWT coefficients in (10) is continuous. In order to reduce computational complexity, a numerical implementation corresponding to the discrete version of the CWT that is distinct from the discrete wavelet transform (DWT) has been applied. The main issue in wavelet analysis is the selection of a mother wavelet. Here the mother wavelet chosen is the bump wavelet with parameters $\mu = 1$ and $\sigma = 0.1$ since it allows a good frequency resolution, because an orthogonal function avoids redundant coefficients. As stated before, the scalogram is not a representation on the time-frequency plane, but rather on the time-scale plane. Thus to achieve a clearer analysis we proceeded to the conversion between scales and frequencies through the use of pseudo-frequencies as already described in Pugliano et al. (2016).

The multipath error central frequency is proportional to the orthogonal distance from the antenna to the reflecting plane, inversely proportional to the wavelength and is a function of the satellite elevation angle as could be seen in (12)

$$f = \frac{2d}{\lambda_i}\sin(\beta)|\dot{\beta}| \tag{12}$$

where d is the distance of reflector, β is satellite elevation, $\dot{\beta}$ the elevation rate and λ_i is the wavelength of the signal. By observing (12), even if reflectors are the same, the multipath central frequency could be different depending on the elevation angle of the considered satellite.

In this work, CWT analysis has been conducted for all visible satellites in each site. Here we discuss a subset. Below the analysis for PRN 08 (Fig. 11) and PRN 14

Table 5 Galileo and GPS satellite code multipath time frequency analysis

Satellite	Block type	Signal	Epoch (Second of day)	Elevation (Deg)	Azimuth (Deg)	Central freq. (mHz)	Power (mW)
PRN 08	Galileo FOC	E1	7285	37.78	14.89	185.2	120.4
PRN 01	GPS IIF	L1	25,370	37.22	12.86	213.4	90.7
PRN 24	GPS IIF	L1	67,339	37.61	15.74	213.4	132.7

(Fig. 13), satellites in RGDG site are reported, whose time domain analysis has been documented in Figs. 4 and 5. The temporal information assumes strong evidence by conducting this analysis over 3 days.

By observing Fig. 11, it appears that the energy peaks are centered around 200 mHz at well-defined time instants: 7300 s in the lower box, 4800 s in the middle box and 2400 s in the upper box, confirming the peaks repeat themselves periodically every 10 days.

By observing Fig. 12, it appears that the PRN 08 satellite is rising, so the elevation angle increases. According to Eq. (12), the frequency of the multipath has to increase. Time frequency analysis, correctly highlights this. In fact, by observing Fig. 11, you can notice how the colored lines are slightly inclined, so the conducted analysis shows that the multipath frequency increases as time increases as expected.

In Fig. 13, the scalograms for PRN 14 satellite are shown for DOY 319 (lower box) and DOY 339 (upper box) in RGDG site. By observing the figure, it appears that energy peaks are centered around 140 mHz at well-defined time instants: 22400 s in the lower box, 17,400 s in the upper box. The figure clearly shows that multipath error peaks occur after 20 days with an advance of approximately 5000 s, as expected.

From Fig. 13, we can see that the frequency is of 140 mHz for PRN 14 satellite while from Fig. 11, it emerges that in RGDG site, the multipath frequency is 200 mHz for PRN 08 satellite. This behavior is due to the greater elevation of the PRN 08 satellite compared to that of PRN 14 satellite at the time instant when the peak occurs. The peaks shown in Figs. 11 and 13 have the same color, meaning that the energy associated to each peak is the same.

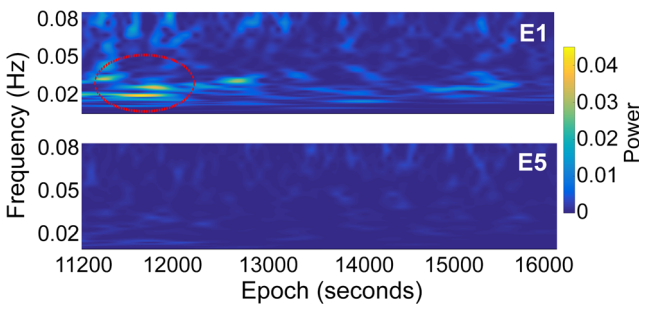

Fig. 16 E1 and E5 multipath estimation bump CWT scalogram for the Galileo PRN 24 satellite in HARB site for DOY 319. The red circles highlight code multipath for the E1 signal. Galileo E5 signal shows very low-multipath error

Galileo multipath performances are compared with those of GPS also in the time-frequency plane. The advantage of wavelet analysis is highlighted in the comparison between Galileo and GPS in the time-frequency plane. The wavelet analysis was performed at first on the Galileo satellites, allowing to identify the instant in which multipath occurred. As for the Galileo PRN 08 satellite at RGDG site on November 14, 2016 (DOY 319) from the identification of the time instant it was possible to obtain the exact satellite azimuth and elevation. Subsequently we conducted a research to find a GPS satellite with the same elevation and azimuth. This research enabled us to identify two GPS satellites in that exact position (PRN 01 and PRN 24), which were also analyzed in the time-frequency domain. This enabled us to compare the results of the two systems. Figures 14 and 15 show the time-frequency analysis on two pairs of satellites with the same azimuth and elevation: GPS PRN 01-Galileo PRN 08 and GPS PRN 24-Galileo PRN 08. The comparison was made between L1 GPS and E1 Galileo signals.

In the first row of Fig. 14 are reported GPS PRN 01 and Galileo PRN 08 code multipath observable plotted versus time expressed in seconds of day. The respective scalograms are reported in the second row. In order to make a comparison, the two satellites have the same azimuth (about 15 degrees) and elevation (about 37 degrees). By observing the first row it can be noticed that multipath error for GPS satellite is noisier than Galileo. This is evident also in time frequency representation. By observing the scalograms of Fig. 14, we can identify a peak for each satellite. For GPS PRN 01 satellite other zones with significant power appear in the range 26,500–28,000 s according to the multipath observables showed in the first row. It can also be noticed that the frequency of the multipath decreases for GPS PRN 01 and increases for Galileo PRN 08 satellite: according to the Eq. (12), the frequency values follow the red line which represents a scaled version of the satellite elevation. This representation gives the opportunity to identify the central frequency, the power associated to the peak and the time instant. The same analysis has been carried on satellite pair GPS PRN 24-Galileo PRN 08 and the results are shown in Fig. 15.

A complete resume of the values of this time-frequency analysis is reported in Table 5. The peak multipath occurs at 213 mHz for GPS and 185 mHz for Galileo. This difference confirms the theoretical frequency model that shows a direct proportion between the multipath frequency and the satellite

elevation rate: in fact, the difference is only due to the lower Galileo satellite elevation rate $\dot{\beta}$ since the measurements were made using the same receiver-antenna couple, the satellites are at the same azimuth and elevation.

In Fig. 16, the E1 and E5 multipath scalograms are plotted for November 14, 2016 (DOY 319). By observing the two rows a comparison between E1 and E5 code multipath error for the Galileo PRN 24 satellite in HARB site can be done.

As can be seen, the Galileo E5 signal is able to reduce code multipath drastically: the error for the E1 signal centered at 20 mHz shown in the first row disappears in the E5 signal scalogram in the second row. This is yet another confirmation of the excellent performance of the E5 signal with respect to multipath.

Conclusion

We showed the results of the pseudorange code multipath error analysis for the Galileo FOC E1, E5a, E5b, and E5 1 Hz data in six sites over 3 days, particularly a time-frequency analysis has been performed. The procedure involves the use of code-minus-carrier (CMC) and pseudorange multipath (MP) observables. The multipath central frequency has been assessed by using the CWT time-frequency analysis. We have shown that the time-frequency technique can be applied directly at the GNSS sites for multipath investigation purposes. CWT allows to properly identify the time instants in which multipath occurs, its central frequency and the associated energy. Such results, in terms of both time and frequency, cannot be achieved with other analysis tools and are relevant for the characterization of the multipath environment. Satellite elevation and azimuth at a given time instant are known, thus it could be possible to identify the direction in which multipath source is located. In addition, if the single ray multipath model can be considered valid, the distance of the multipath source from the antenna can be calculated using the frequency identified by using Eq. 12.

Through our analysis, we can conclude that the expectations of FOC satellites to provide improvement of the multipath performance have been verified, obtaining results which are in line with some other researches presented by Simsky et al. (2006) on the observations of GIOVE and, more recently, by Zaminpardaz and Teunissen (2017). In more detail the results bring to the following conclusions: (1) the E5 signal shows a significant suppression of multipath as compared to the other Galileo and GPS signals and it is almost independent of the satellite elevation showing a stable performance; (2) at low elevations the E1 signal has the highest multipath compared to the other Galileo signals; (3) the difference among the multipath performance of Galileo codes (E1, E5a, E5b, E5) is more evident at low elevations while at high elevations all Galileo signals show similar values of multipath errors; (4) the effect on the multipath performance of different antenna sites are similar at high elevations; (5) at a specific site, an assigned FOC satellite showed a lower frequency multipath compared to a GPS satellite, at the same azimuth and elevation, according to the theoretical frequency model (Leick 2004) that shows a direct proportion between the multipath frequency and the satellite elevation rate: the Galileo satellite elevation rate is in fact lower than the GPS one.

References

Aram M, El-Rabbany A, Krishnan S, Anpalagan A (2007) Single frequency multipath mitigation based on wavelet analysis. Navigation 60(2):281–290

Bartone C, Zhang Y (2005) Real-time wavesmooth error mitigation for Global Navigation Satellite Systems. United States Patent Application Publication No. US 2005/0212696 A1

Blanco-Delgado N, de Haag MU (2011) Multipath analysis using code-minus-carrier for dynamic testing of GNSS receivers. In: Proceedings of ICL-GNSS 2011, Tampere, Finland, pp. 25–30

Borio D, Lo Presti P (2008) Data and pilot combining for composite GNSS signal acquisition. International journal of navigation and observation, volume 2008, 12 pages

Braasch MS (1996) Multipath Effects. Global positioning system: theory and applications, vol I. American Institute of Aeronautics and Astronautics, Washington, DC, pp 547–568

Changsheng C, Chang H, Rock S, Lin P, Xianqiang C, Jianjun Z (2016) A comparative analysis of measurement noise and multipath for four constellations: GPS, BeiDou, GLONASS and Galileo. Surv Rev 48(349):287–295

Circiu MS, Meurer M, Felux M, Gerbeth D, Thölert S, Vergara M, Enneking C, Sgammini M, Pullen S, Antreich F (2017) Evaluation of GPS L5 and Galileo E1 and E5a performance for future multifrequency and multiconstellation GBAS. Navigation 64(1):149–163

de Bakker P, van der Marel H, Tiberius C (2009) Geometry-free undifferenced, single and double differenced analysis of single frequency GPS, EGNOS and GIOVE-A/B measurements. GPS Solutions 13(4):305–314

de Bakker P, Tiberius C, van der Marel H, van Bree R (2012) Short and zero baseline analysis of GPS L1 C/A, L5Q, GIOVE E1B, and E5aQ signals. GPS Solutions 16(1):53–64

Defraigne P, Bruyninx C (2007) On the link between GPS pseudorange noise and day-boundary discontinuities in geodetic time transfer solutions. GPS Solutions 11(1):239–249

Diessongo H, Schuler T, Junker S (2014) Precise position determination using a Galileo E5 single-frequency receiver. GPS Solutions 18(1): 73–83

Dow JM, Neilan RE, Rizos C (2009) The International GNSS service in a changing landscape of global navigation satellite systems. J Geod 83(3):191–198

El-Rabbany A (2002) Introduction to GPS: the global positioning system. Artech House, Boston London

Estey LH, Meertens CM (1999) TEQC: the multi-purpose toolkit for GPS/GLONASS data. GPS Solutions 3(1):42–49

Hakansson M, Jensen A, Horemuz M, Hedling G (2017) Review of code and phase biases in multi-GNSS positioning. GPS Solutions 21(3): 849–860

Hofmann-Wellenhof B, Lichtenegger H, Collins J (2001) Global positioning system: theory and practice, 5th edn. Springer Verlag Wien, New York

Julien O, Lachapelle G, Cannon ME (2004) A new multipath and noise mitigation technique using data/data-less navigation signals. Proc. ION GNSS 2004, Institute of Navigation, Long Beach, California, USA, September 21-24, 8–19

Leick A (2004) GPS satellite surveying, 3rd edn. John Wiley & Sons, New York

Mannucci AJ, Iijima BA, Wilson BD, Peck S, Ahmadi R (1997) Wide area Ionospheric delay corrections under ionospheric storm conditions. Proc. ION NTM 1997, Institute of Navigation, Santa Monica, California, USA, January 14–16, 871–882

Navarro-Reyes D, Castro R, Bosch P (2015) Galileo first FOC launch: recovery mission design 25th International Symposium on Space Flight Dynamics ISSFD October 19–23, Munich, Germany

OS SIS ICD (2015) European GNSS (Galileo) open service, signal in space, interface control document. European Union and European Space Agency (ESA), tech rep, Issue 1.2

Paziewski J, Sieradzki R, Wielgosz P (2018) On the applicability of Galileo FOC satellites with incorrect highly eccentric orbits: an evaluation of instantaneous medium-range positioning. Remote Sens 10:208

Petovello M, Groves P (2013) Multipath vs. NLOS signals. Inside GNSS November–December 2013: 40–44

Pugliano G, Robustelli U, Rossi F, Santamaria R (2016) A new method for specular and diffuse pseudorange multipath error extraction using wavelet analysis. GPS Solutions 20(3):499–508

Satirapod C, Rizos C (2005) Multipath mitigation by wavelet analysis for GPS base station applications. Surv Rev 38(295):2–10

Seepersad G, Bisnath S (2014) Reduction of PPP convergence period through pseudorange multipath and noise mitigation. GPS Solutions 19(3):369–379

Simsky A, Sleewaegen J, Hollreiser M, Crisci M (2006) Performance assessment of Galileo ranging signals transmitted by GSTB-V2 satellites. Proc. ION GNSS 2006, Institute of Navigation, Fort Worth, Texas, USA, September 26-29, 1547–1559

Simsky A, Mertens D, Sleewaegen J, Hollreiser M, Crisci M (2008) Experimental results for the multipath performance of Galileo signals transmitted by GIOVE-A satellite. International Journal of Navigation and Observation, vol 2008

Smith SW (1999) The scientist and engineer's guide to digital signal processing. California Technical Publishing, San Diego

Soloviev A, Kuusniemi H, Bisnath S (2007) Backing up GNSS with laser radar & INS, RAIM in the city, antenna phase wind-up. Inside GNSS July/August pp 32–35

Sosnica K, Prange L, Kazmierski K, Bury G, Drozdzewski M, Zajedel R, Hadas T (2018) Validation of Galileo orbits using SLR with a focus on satellites launched into incorrect orbital planes. J Geod 92:131–148

Souza EM, Monico JFG (2004) Wavelet shrinkage: high frequency multipath reduction from GPS relative positioning. GPS Solutions 8(3): 152–159

Tawk Y, Botteron C, Jovanovic A, Farine P (2011) Analysis of Galileo E5 and E5ab code tracking. GPS Solutions 16(2):243–258

Yates R, Lyon R (2008) DC blocker algorithms. IEEE Signal Process Mag 25(2):132–134

Zaminpardaz S, Teunissen PJG (2017) Analysis of Galileo IOV + FOC signals and E5 RTK performance. GPS Solutions 21(4):1855–1870

Zhang J, Lohan E (2011) Galileo E1 and E5a link-level performances in single and multipath channels. Lecture Notes of the Institute for Computer Sciences, Social Informatics and Telecommunications Engineering (LNICST) 71:378–390